1.0

1.1

1.25   1.4   1.6

4.5   2.8   2.5
5.0   3.2   2.2
5.6   3.6
6.3   4.0   2.0

1.8

MICROCOPY RESOLUTION TEST CHART
NATIONAL BUREAU OF STANDARDS-1963-

LEVEL II

(12)

NORTHWESTERN UNIVERSITY

DEPARTMENT OF MATERIALS SCIENCE

(9) Technical Report No. 23
May 14, 1979

(15) Office of Naval Research
Contract N00014-75-C-0580
NR 031-733

(6) STRESS ANALYSIS FROM POWDER DIFFRACTION PATTERNS.

by

(10) J. B. Cohen, H. Dölle and M. R. James

(11) 14 May 79 (12) 44p. (14) TR-23

DDC FILE COPY

NORTHWESTERN UNIVERSITY
QUAECUMQUE · SUNT · VERA
1851

DDC
RECEIVED
JUN 13 1979
E

EVANSTON, ILLINOIS

260 810   LB

79 06 11 065

STRESS ANALYSIS FROM POWDER DIFFRACTION PATTERNS

by

J. B. Cohen and H. Dölle[o]
Dept. of Materials Science & Engineering
The Technological Institute
Northwestern University
Evanston, IL 60201

and

M. R. James
Science Center/Rockwell International
Thousand Oaks, CA 91360

Abstract

A brief review of the method of measuring residual stresses in poly-crystalline materials with X-rays is given. The effect of counting statistics on precision is discussed as well as factors that affect accuracy. Beam penetration, stress gradients, and the form of the stress tensor can each seriously affect accuracy, if traditional methods are employed, and practical procedures to deal with such situations are outlined.

Accession For		
NTIS GRA&I		☑
DDC TAB		☐
Unannounced		☐
Justification		
By		
Distribution/		
Availability Codes		
Dist	Avail and/or special	
A		

[o]J. B. Cohen is Frank C. Engelhart Professor of Materials Science and
Engineering and H. Dölle is a Post-Doctoral Visiting Scholar.

1. Introduction

Knowledge of stresses (applied or residual) is quite important in an industrial environment. Crack initiation and propagation in static or fatigue loading, or in stress corrosion, can be impeded by compressive stresses normal to the crack, and greatly accelerated by tensile stresses. Residual stresses can be produced during quenching (because of the different cooling rates of the surface and the interior and any volume changes due to transformations), during manufacturing (due to the difference in deformation of the surface and the interior - as in straightening, machining, rolling or shot peening), or due to the different response of particles and matrix in a multiphase material. During welding, the resistance of the cold base metal to the solidifying (and shrinking) weld pool will produce stresses in both regions. These stress patterns can and do change in service, and there is increased interest in monitoring these. For a recent overview, see ref. 1.

Apart from deliberately induced residual stresses, the measured stresses can develop due to applied loads, or even in a quasi-uniform stress field, from differences in response of the surface and the interior, one grain with respect to another, or one phase with respect to another. In the case of residual stresses the tensile and compressive components must balance across a section, but to see this it may be necessary to examine values in different phases. This is possible with X-rays, but it has not often been of sufficient interest; only the stresses in the major constituent are usually examined. Also, even in a single phase material there may be situations where it is not possible to remove material to examine gradients because of the geometry of the piece.

Actually, a variety of non-destructive techniques, based on the acoustic and magnetic response of a material to stresses, are being evaluated for this purpose, but so far they have proved to be too sensitive to microstructural

variations such as changes in texture[2]. The X-ray method, which was first proposed in the 1920's by Lester and Aborn[3], has withstood the test of time in industry; it is the subject of this review, in which we shall examine not only the method, but its limitations, accuracy and precision, as well as the latest developments which have made it of considerable use in field situations. While there are a number of ways of examining strains with X-rays, we shall concentrate only on those that are widely employed in industry. To prove their validity, these approaches have been compared to measurements of distortion after mechanical dissection[1].

The basic principle that is employed is quite simple: An interplanar spacing (d) in the material serves as an internal strain gauge. As shown in Fig. 1a, in a polycrystalline specimen in the normal position on a diffractom-eter, only those grains with planes nearly parallel to the surface form a dif-fraction peak. If there are compressive stresses in the near-surface regions, the "d" spacing is increased for these planes due to the effect of Poisson's ratio. When the specimen is tilted with respect to the X-ray beam (or the beam to the specimen), Fig. 1b, the diffracting grains have their planes more nearly perpendicular to the stresses in the surface and their spacing is less, or even decreased. (Components of the surface stress parallel and perpendicular to the planes now affect this spacing.) The 2θ positions of diffracting peaks from such planes and Bragg's law are all that are required to examine the strain tensor, from which the surface stresses may be determined.

2. The Basic Equation

In what follows, we shall employ the axial system, $\underline{L}_i$, for the measurements (a "laboratory" system) and axes $\underline{P}_i$ for the specimen, as shown in Fig. 2. Primed quantities will refer to measurements in the laboratory system, unprimed in the sample system. With $d_{\Phi\psi}$ the interplanar spacing at tilts Φ, ψ and d_o the

value for the strain free material, the strain along L_3 can be written[4]:

$$\epsilon'_{33} = \frac{d_{\Phi\psi} - d_o}{d_o} = \epsilon_{11}\cos^2\Phi\sin^2\psi + \epsilon_{12}\sin2\Phi\sin^2\psi + \epsilon_{13}\cos\Phi\sin2\psi + \epsilon_{22}\sin^2\Phi\sin^2\psi$$

$$+ \epsilon_{23}\sin\Phi\sin2\psi + \epsilon_{33}\cos^2\psi. \tag{1}$$

Once the strains are determined (by the procedures to be described below), the stresses, σ_{ij}, can be calculated from:

$$\sigma_{ij} = \frac{1}{\frac{1}{2}S_2(hk\ell)}\left[\epsilon_{ij} - \delta_{ij}\frac{S_1(hk\ell)}{\frac{1}{2}S_2(hk\ell)S_1(hk\ell)}(\epsilon_{11} + \epsilon_{22} + \epsilon_{33})\right]. \tag{2}$$

The term δ_{ij} is the Kronecker delta function, and since $\delta_{ij} = 0$, $i \neq j$; the shear strains alone determine the shear stresses.

The S_i are X-ray elastic constants for a particular hkℓ reflection. For an elastically isotropic solid, $\frac{1}{2}S_2(hk\ell) = \frac{(1+\mu)}{E}$, $S_1(hk\ell) = (\frac{\mu}{E})$, where μ is Poisson's ratio and E is Young's modulus. Theory exists to calculate the constants (for each hkℓ reflection) for an anisotropic crystal coupled to an isotropic matrix, and this theory shows that the values are within a few percent of the average of the well known Reuss and Voight formulae, which assume, respectively, constant average stress and constant average strain for all grains in the material. In addition, theory is developing for an elastically anisotropic material with severe texture. (This entire area has recently been reviewed by one of us, Ref. 5.) In the latter case, the elastic constants associated with a particular hkℓ reflection may vary with Φ and ψ tilt. It has also been well established that the X-ray elastic constants can vary appreciably with amount of plastic deformation; changes as large as 20-40 pct. have been reported. This phenomenon is not understood at the moment and can obviously severely affect the accuracy of any stress measurement if calculated values are assumed to be independent of prior strain. Fortunately, it is possible to

test for this problem, and, in many cases, to measure the effective constants. We discuss this further below. In addition, it is often the relative change in stress with some change in condition that is important, in which case the constants employed are not as important.

We turn now to the various methods, after which we will discuss other errors that affect accuracy, and also precision.

3. Surface Stresses Only

As a free surface cannot support a stress normal to it ($\sigma_{33} = \sigma_{13} = \sigma_{23} = 0$), the stress tensor in the <u>sample</u> system shown in Fig. 2 is:

$$\begin{pmatrix} \sigma_{11} & \sigma_{12} & 0 \\ \sigma_{12} & \sigma_{22} & 0 \\ 0 & 0 & 0 \end{pmatrix} . \tag{3a}$$

Of course, this tensor may be written in terms of principal axes in a rotated axial system:

$$\begin{pmatrix} \sigma_1 & 0 & 0 \\ 0 & \sigma_2 & 0 \\ 0 & 0 & 0 \end{pmatrix} . \tag{3b}$$

Then, it can be shown that:

$$\epsilon'_{33} = \frac{d_{\Phi\psi} - d_o}{d_o} = \frac{1}{2} S_2(hk\ell)[\sigma_1 \cos^2\Phi + \sigma_2 \sin^2\Phi]\sin^2\psi + S_1(hk\ell)[\sigma_1 + \sigma_2]. \tag{4}$$

Note that at $\psi = 0^o$, a comparison of $d_{\Phi\psi}$ to d_o immediately indicates whether the sum of the principal stresses is positive or negative.

Subtracting the value for $\psi = 0^o$:

$$\left(\frac{d_{\Phi\psi} - d_o}{d_o}\right) - \frac{d_{\Phi, \psi=90^o} - d_o}{d_o} \cong \frac{d_{\Phi\psi} - d_{\Phi, \psi=0}}{d_{\Phi, \psi=0}}$$

$$= \frac{1}{2} S_2(hk\ell)\sigma_\Phi \sin^2\psi. \tag{5}$$

The stress in any direction, Φ, on the surface can be determined simply from the slope of d vs $\sin^2\psi$. The stress-free value, d_o, is not needed. A typical plot is shown in Fig. 3. The principal stresses and their directions can be obtained[6], although their Φ directions are often known from the nature of the applied stress system. By application of known elastic stresses on an identical specimen, the effective elastic constants can be obtained from Eqns. 4 or 5.

It cannot be emphasized too strongly that the linearity of "d" vs. $\sin^2\psi$ must be confirmed in each situation, but if this is the case, the equation can be further simplified, with the aid of Bragg's law, to involve only two tilts, $\psi = 0°$ and, typically, $\psi = 45°$ or $60°$:

$$\sigma_\Phi = K\Delta 2\theta \text{ (in degrees)}, \tag{6a}$$

with:

$$K = \frac{\pi}{180} \quad \frac{1}{S_2(hk\ell) \sin^2\psi} \cot[\tfrac{1}{2}(\theta_{\psi=0} + \theta_{\psi=\psi})]. \tag{6b}$$

In this "two exposure method," a high angle peak is chosen, and the ψ tilt is made as large as possible, to minimize K and hence maximize the sensitivity of the peak shift to the stress. For example, for steel, CrK_{α_1} radiation, the 211 reflection at $\approx 156°2\theta$, and a ψ-tilt of $45°$, a $+ 0.1°2\theta$ shift corresponds to a stress of ≈ -60 MPa (-8600 psi). Shifts as small as $0.01 - 0.02°2\theta$ can be detected. If it has been verified that d vs $\sin^2\psi$ is indeed linear, it is possible to develop simple portable equipment (for use in the field, or in a factory environment) which can measure the surface stress in seconds. An example of this equipment is shown in Fig. 4[7]. It is even possible to use only one incident beam direction and examine, simultaneously with two detectors, two points on the diffraction cone which come from grains tilted at different ψ values[8]. However, it has been shown[1] that in this case the stress constant,

K, is much larger, which implies a larger error in stress from a given uncertainty in 2θ. (Film equipment employing this "single exposure" technique is still sometimes used for very large pieces.)

Because of the simple form of Eqn. 6a, it is particularly easy to measure K by applying a series of known elastic loads to a specimen. Tensile or bending loads are commonly employed[9,10].

4. The General Stress State

Because the measured stresses are averages over a finite depth of beam penetration, we should consider the general stress tensor:

$$\begin{pmatrix} \sigma_{11} & \sigma_{12} & \sigma_{13} \\ \sigma_{12} & \sigma_{22} & \sigma_{23} \\ \sigma_{13} & \sigma_{23} & \sigma_{33} \end{pmatrix} . \tag{7}$$

Referring to Eqn. 1, the presence of ϵ_{13} and ϵ_{23} leads to curvature in the d vs $\sin^2\psi$ relationship, as their contribution depends on $\sin 2\psi$. Such terms can be important in machining, or in wear; that is, when there are strong components of the deforming forces tangential to their surface, and strong gradients (since the strains ϵ_{13}, ϵ_{23}, ϵ_{33} must vanish at the surface). Examples of this effect (from ref. 11) are shown in Figs. 5 and 6. The principal effect of the shear stresses is to cause "d" vs $\sin^2\psi$ to be non-linear in opposite senses for positive and negative ψ tilts. This ψ splitting and the large curvature near $\psi=0$ are distinguishing features of this phenomenon. The actual stress tensors are given in the captions to the figures, and the small value of the shear stress to cause the "ψ splitting" is particularly noteworthy. Also, the curves for positive and negative ψ (or by changing ϕ by 180°) reverse when the sign of the shear stress reverses, Fig. 6. This curvature and its cause were first reported by Walburger[12], and a simple method of analysis of the data was suggested by

Dölle and Hauk[12]. It was employed in an extensive study for the first time by Dolle and Cohen[11], introducing the terms a_1 and a_2, employing Eqn. 1 and using carats to indicate averages over the depth of penetration:

$$a_1 \equiv \tfrac{1}{2}[\epsilon_{\Phi\psi+} + \epsilon_{\Phi\psi-}] = \langle\epsilon_{33}\rangle + [\langle\epsilon_{11}\rangle\cos^2\Phi + \langle\epsilon_{12}\rangle\sin 2\Phi + \langle\epsilon_{22}\rangle\sin^2\Phi - \langle\epsilon_{33}\rangle]\sin^2\psi,$$

$$\tag{8a}$$

$$a_2 \equiv \tfrac{1}{2}[\epsilon_{\Phi\psi+} - \epsilon_{\Phi\psi-}] = [\langle\epsilon_{13}\rangle\cos\Phi + \langle\epsilon_{23}\rangle\sin\Phi]\,\sin|2\psi|. \tag{8b}$$

Thus, $\langle\epsilon_{33}\rangle$ can be obtained from the intercept of a_1 vs $\sin^2\psi$; this value is independent of Φ, and so it can be verified by measurements at different Φ tilts. The components ϵ_{11}, ϵ_{12}, ϵ_{22} can be obtained from $\partial a_1/\partial\sin^2\psi$. At $\Phi = 0°$, $\epsilon_{11} - \epsilon_{33}$, and hence ϵ_{11}, is obtained, whereas for $\Phi = 90°$, ϵ_{22} can be measured. The ϵ_{12} component is then determined from $\left[\dfrac{\partial a_1}{\partial\sin^2\psi}\right]_{\Phi=45°}$. From $\dfrac{\partial a_2}{\partial\sin|2\psi|}$, ϵ_{13} is calculated for $\Phi = 0°$, ϵ_{23} for $\Phi = 90°$. The curves in Figs. 5 and 6 are the fit to the data points with Eqn. 1.

The stresses are then obtained from Eqn. 2.

In this procedure, it _is_ necessary to know "d_o." For steels, measurements generally yield a value for the lattice parameter of 2.8665(1) Å. The uncertainty leads to a change of $\approx \pm$ 30 MPa in the normal stresses and hardly any variation in the shear stresses. Measurements with a well annealed powder of Cr indicate that the precision is 15 MPa for σ_{11}, σ_{12}, σ_{22}, σ_{33}, and better than 8 MPa for σ_{13}, σ_{23}. This uncertainty is often less than the variation of the actual stresses from point to point in a specimen.

Another way of examining the stress in three dimensions is with high-energy X-rays or neutrons, isolating the volume element to be examined by suitably narrowing the slits defining the incident and diffracted beams. The feasibility of such a procedure is considered in the next paper.

Except for materials with appreciable content of a second phase (such as a steel with more than ≈ 0.4 wt. pct C), some kinds of deformation may produce strong texture at modest strains. In such cases oscillations have been observed in d vs $\sin^2\psi$ as shown in Fig. 7. The precise interpretation for this effect is still uncertain; it may be due to elastic or plastic aniso-tropy[-,5]. Tests are currently underway to decide which factor is most im-portant, after which procedures may be possible to minimize this problem. For exam-ple, any contributions from elastic anisotropy can be minimized (for any materi-al) by employing hoo or hhh reflections[5].

5. Gradients

The ability to detect stresses normal to the surface, as was discussed in the previous section, is based on the presence of gradients, and the fact that the X-ray beam averages over its penetration (D). Therefore, it is appropriate to examine the effects of such gradients because, even in the absence of stresses normal to the surface, there will be effects on $\langle\sigma_{11}\rangle$, $\langle\sigma_{22}\rangle$, $\langle\sigma_{12}\rangle$. Correc-tions are available for this[1,5], and also for stress relief due to layer removal[1], if the gradients are examined in this fashion. But the presence of steep gradients can also be detected and examined from the form of "d" vs $\sin^2\psi$ without layer removal, as illustrated in Fig. 8. For this figure, the stresses were obtained from an assumed stress profile (in the z-direction)[5]:

$$\langle\sigma_{ij}\rangle = \sigma_{ij}(z{=}0) + \int_0^D \exp(-z/\tau)g_{ij}(z)dz. \tag{9}$$

Here, with μ the linear absorption coefficient:

$$\tau = \frac{\sin^2\theta - \sin^2\psi}{2\mu\sin\theta\,\cos\psi}, \tag{10a}$$

for ψ tilts around the θ axis, and:

$$\tau = \frac{\sin\theta\,\cos\psi}{2\mu}, \tag{10b}$$

for tilts around an axis parallel to the plane of the diffractometer. The term $g_{ij}(z)$ describes the variation of stress with depth (z) below the surface. (Once these average stresses are evaluated for a particular strain distribution $\langle \epsilon'_{33} \rangle$ can be calculated at each ψ and d vs. $\sin^2 \psi$ obtained as will be shown below.

Note particularly the difference in curvature near $\psi = 0$ between this effect (if shear stresses $\langle \sigma_{13} \rangle$, $\langle \sigma_{23} \rangle = 0$) and for ψ splitting (compare Fig. 8 with Figs. 5 or 6). Also, the values of d at $\pm \psi$ should be identical in this case, so the effect is readily distinguished from ψ splitting.

This curvature can be employed to obtain information about gradients, and we now present a concrete example of how this can be done, with data from a SAE 1040 steel, normalized and shot peened. We make the following assumptions (all of which could be checked in a more thorough investigation):

a) the X-ray elastic constants S_1 and S_2 do not vary with depth, z:

b) σ_{ij} varies with z only;

c) $\Phi = 0^{\circ}$(by definition)

d) $\sigma_{11}(z) = \sigma_{22}(z)$ (due to shot peening normal to the surface);

e) $\sigma_{ij}(z)$, $i \neq j = 0$ (no appreciable shear deformation).

Then:

$$\langle \epsilon'_{33} \rangle_{\Phi=0} = \tfrac{1}{2} S_2 (hk\ell) [\sin^2 \psi \langle \sigma_{11} \rangle + (1 - \sin^2 \psi) \langle \sigma_{33} \rangle] + S_1 (hk\ell) [2 \langle \sigma_{11} \rangle + \langle \sigma_{33} \rangle].$$

$$(11)$$

From this equation:

$$\langle \epsilon'_{33} \rangle_{\Phi, \psi=0} = 2 S_1 (hk\ell) \langle \sigma_{11} \rangle + \langle \sigma_{33} \rangle [\tfrac{1}{2} S_2 (hk\ell) + S_1 (hk\ell)], \qquad (12a)$$

$$\frac{\partial \langle \epsilon'_{33} \rangle_{\Phi=0}}{\partial \sin^2 \psi} = \tfrac{1}{2} S_2 (hk\ell) [\langle \sigma_{11} \rangle - \langle \sigma_{33} \rangle]. \qquad (12b)$$

With Eqns. 12, first estimate of $\langle \sigma_{11} \rangle$ and $\langle \sigma_{33} \rangle$ can be obtained, fitting a straight line to the data. Typical data is shown in Fig. 9. From this figure,

these first estimates are: $\langle\sigma_{11}\rangle$ = -309 MPa, $\langle\sigma_{33}\rangle$ = 140 MPa. Comparison of Fig. 9 with Fig. 8 assuming the gradients are linear indicates that either $g_{11} < 0$ or $g_{33} > 0$, or both.

The measured macroscopic gradient is illustrated in Fig. 10a. It can be seen that the stresses vanish at $\approx$ 500 μm. A simple representation of this figure was taken to be Fig. 10b. The terms z_2 and g_{ij} were varied to give the best fit to the data : $\langle\sigma_{11}\rangle$, $\langle\sigma_{33}\rangle$, and the measured slopes of "d" vs $\sin^2\psi$ at various ψ angles.

From the average $\langle\sigma_{33}\rangle$ = 140 MPa and the penetration depth, τ = 10 μm, g_{33} was the order of 15 MPa. From the curvature of "d" vs $\sin^2\psi$ it could be concluded that g_{11} was -10 to -15 MPa/μm. These values were actually obtained simply by choosing various z_2 values and surface stresses. Of course, more sophisticated least-squares approaches are possible. This procedure might be particularly fruitful when many similar samples have to be examined for their gradients, and the gradient in one specimen has been measured by layer removal.

Finally, it is worth noting that peak shapes, as well as positions have been employed by Murakami[14] to obtain information on gradients in thin foils. While his assumptions as to the stress tensor are too restrictive for general use, his procedure could be expanded.

6. Factors Affecting Accuracy

We have already mentioned one possible source of inaccuracy, the elastic constants. The actual error in stress from the effects to be discussed below can be evaluated through the stress constant K and Eqns. 6, or by employing experimental X-ray elastic constants S_1 and S_2. A particular error in 2θ, when multiplied by K for the chosen material, gives a first estimate of the error in stress.

All data should be corrected for the variation in scattering factor and Debye-Waller factor if the peak is very broad ($> \approx 5^{\circ}$ in half breadth). Corrections for the Lorentz polarization and absorption factors (LPA) can be written for each position, 2θ, across a peak. Assuming filtered radiation:

$$\text{LPA} = \frac{1 + \cos^2 2\theta}{\sin^2 \theta} \, (1 - \tan\psi \, \cot\theta), \tag{13a}$$

for tilts around the 2θ axis, and:

$$\text{LPA} = \frac{1 + \cos^2 2\theta}{\sin^2 \theta} \, , \tag{13b}$$

for tilts around an axis parallel to the goniometer. The latter method[15,16] is increasingly employed in Europe. It is not limited to $|\psi| \leq \theta$, as is a tilt around the θ axis. Furthermore, the path lengths of the incident and diffracted beams within the specimen are equal, so absorption corrections are not involved (Eqn. 13b vs Eqn 13a). It is a helpful technique for measurements in difficult locations such as on gear teeth, where the incident or diffracted beam can be blocked by the gear itself.

Because these corrections are small and straightforward there is no need to avoid them, and therefore no need to estimate errors from these sources.

Locating the specimen over the center of rotation can be particularly troublesome especially when the geometry of the specimen is complicated and this is one of the largest sources of inaccuracy. There are two ways of achieving this location. The lattice parameter for two or more different reflections (widely separated in 2θ) can be plotted vs $\frac{\cos^2 \theta}{\sin\theta}$. Then (for $\psi = 0^{\circ}$), with "a" the lattice parameter[17]:

$$\frac{\Delta a}{a} = -\frac{2\delta}{R} \, \frac{\cos^2 \theta}{\sin\theta} \, , \tag{14}$$

with δ the sample displacement and R the goniometer radius. The displacement can therefore be calculated from the slope of such a plot, and the sample

displaced appropriately.

Another way, particularly important when ψ splitting is suspected, is to examine the peak position of a stress free powder (painted in a thin layer on the specimen in an acetone solution) at a fixed 2θ (close to the reflection angle of the specimen) and then varying ψ. An example of such a method is shown in Fig. 11.

In Japan, a parallel beam method is employed[18], to eliminate the sensitivity to sample position. In Fig. 12, a comparison of the peak shift due to sample displacement is made between this method, the parafocussing method (for which, the receiving slits are moved to the correct focus at each ψ), and a stationary slit, divergent beam. The parallel beam technique is obviously least sensitive. However, the peak is broadest in this case and the time for data analysis is $\approx$ 1/3 longer for the same statistical error (Section 7) than parafocussing, and the reproducibility twice as poor for sharp profiles[19]. The stationary slit method appears to be the best compromise. However in this case (but not in parafocussing) the shape of the peak may vary with ψ tilt. How this alters various methods for peak location is illustrated in Fig. 13. Bias corrections may be taken from this plot.

(If parafocussing is employed, and the sample has a strong texture, it is important to introduce a permanently fixed slit, defining the beam, along the θ axis; it is not moved when the scanning slit is moved to the correct focus. This assures that the same portion of the diffraction cone is seen at all ψ tilts[20].)

An excellent presentation of the bias from various instrumental misalignments can be found in ref. 2; while the equations in this reference are based on the center of gravity of a peak, they can be used as a guide for any definition of the peak. Another source of analytical approximations to the errors is ref. 22.

For this paper, we have made computer calculations of the peak shifts by a ray-tracing method. The intensity of the beam was assumed to be uniform across its cross section. This over-emphasizes the error and the resultant shifts were multiplied by 1/3, in agreement with the findings in similar comparisons by Zantopulos and Jatczak[13]. The errors summarized in Table I are the shift in 2θ for a ψ tilt from +45° to -45°. If only +ψ is employed, the errors are reduced by an additional factor of 1/2. This table can serve as a quick guide to the important aspects in alignment of the diffractometer for stress determinations. Table II gives some typical errors for the two-tilt method and parafocussing, with tilt around the θ axis. Clearly, the bias due to geometric errors can be held to quite small values, with good alignment and a judicious choice of slits.

7. Factors Affecting Precision

Automation of stress measurements has been achieved in several locations. One such program, for example, includes sample alignment over the tilt axis, and preliminary scans to locate the peak and to determine the time to achieve an operator-specified precision[19,24]. Such on-line controls allow studies to be made of factors affecting reproducibility.

As shown in Table II the error in determining a peak's location is one of the largest sources of uncertainty in the results. A number of methods have been presented to define the angle of diffraction, 2θ, from the diffraction profile, including the apex of a parabola or cubic polynomial fit to the upper portion of the profile[25], the centroid[26] and the half value breadth[18]. Comparisons between these methods indicate that the apex of a least squares parabola fit to that portion of the profile above 85% of the maximum intensity usually provides the most reproducible procedure for defining the diffraction

profile when determining peak shifts[19,24]. This is shown in Table III.

If the intensity I_j accumulated at each jth interval in 2θ is taken at $2n+1$ observation points (the center point being defined as the working origin $2\theta_o$) in equal increments, δ, of 2θ, the peak location in a parabolic fit is given by[24]:

$$2\theta_p = 2\theta_o - (n_2^2 - n_o n_4)\delta^2 M_1 / 2n_2(n_2\delta^2 M_o - n_o M_2),$$ (15a)

where:

$$n_i = \sum_{j=-n}^{n} j^i \text{ and } M_i = \delta^{i+1} \sum_{j=-n}^{n} j^i I_j.$$ (15b)

(Angular intensity corrections such as the Lorentz polarization and absorption factors must be performed on the raw data before determining the peak position.)

Scatter in the peak position arises from statistical fluctuations in the X-ray intensities and the precision of the measured value is properly evaluated by its standard deviation due to counting statistics. The standard deviation in peak location (Eqn. 15) due to the random counting errors is[19,24]:

$$S(2\theta_p) = \left[\frac{\delta^4 (n_2^2 - n_o n_4)^2}{4n_2^2 (n_2\delta^2 M_o - n_o M_2)^4} \sum_{j=-n}^{n} (n_o\delta^3 M_1 j^2 + (n_2\delta^2 M_o - n_o M_2)\delta^2 j \right.$$

$$\left. - n_2\delta^3 M_1)^2 S^2(I_j) \right]^{\frac{1}{2}},$$ (16)

where the variance in the power, $S^2(I_j)$ depends on the method of data accumulation and is given by:

$$S_{FT}^2(I_j) = I_j/t \qquad \text{for fixed time, t,}$$ (17a)

$$S_{FC}^2(I_j) = I_j^2/c \qquad \text{for fixed counts, c.}$$ (17b)

The error, $S(2\theta_p)$, introduces an error in the calculated interplanar spacing given by:

$$S(d) = \left[\frac{\lambda\cos\theta}{2\sin^2\theta}\right]\frac{S(2\theta_p)}{\sqrt{2}}\left(\frac{\pi}{180}\right), \tag{18}$$

where λ represents the characteristic wavelength and $S(2\theta)$ is in degrees 2θ.

The subsequent statistical counting error in measured residual stress is:

$$S(\sigma_\phi) = \left[\frac{\sum_\psi (\sin^2\psi - \overline{\sin^2\psi})^2 \cdot S^2(d\psi)}{[\sum_\psi (\sin^2\psi - \overline{\sin^2\psi})^2]^2}\right]^{\frac{1}{2}} \bigg/ [d_o \cdot S_2^{(hk\ell)}\!/2], \tag{19}$$

for the $\sin^2\psi$ technique (Eqn. 5) and:

$$S(\sigma_\phi) = K[S^2(2\theta_o) + S^2(2\theta_\psi)]^{\frac{1}{2}}, \tag{20}$$

for the two tilt method (Eqn. 6).

Fig. 14a shows the distribution of errors in a large number of actual measurements when $0.01^\circ 2\theta$ was chosen as the desired statistical precision for each peak in a control program employing the above equations. The half-width of the distribution is only $2.4 \cdot 10^{-3}\,^\circ 2\theta$. But when the distribution of errors in repeated measurements on the same specimens was examined (without moving it), the results in Fig. 14b were obtained. Clearly, the scatter is greater than the statistical error. In a series of experiments[19,24], the factors required to achieve reproducibility equivalent to the statistical error were examined. The results can be summarized as follows:

a) Unless the peak is very sharp, at least 7 points should be employed in a parabolic fit, if the two-tilt method is employed - not the three points usually taken. (The total measuring time can be kept fixed.)

b) If the peak-to-background ratio is low (2:1) or the peak is broad (2° or more), background subtraction is required, at least in the first scan to determine the region of fit. (This was not done for the data in Fig. 14,

and this is the main reason for the greater than expected precision.)

Even with (a) and (b) the scatter may be twice that predicted by the above statistical analysis for the two-tilt procedure. But:

c) With the total time kept fixed, the $\sin^2 \psi$ method, with at least a three point parabolic fit and background subtraction will achieve the expected error.

d) An alternative to (c) is to employ a position sensitive detector (PSD) and 30 or more points in the region of fit. In this case, background subtraction is not necessary.

Automation alone will reduce the time of measurement by ≈ 2. A PSD will result in time saving of a factor of 5 or more[24,27]. Indeed if an error of 34 MPa (5 ksi) is acceptable, it has been shown that in some cases measurements can be completed with the two tilt method with 2 seconds for each tilt[7].

Finally it is instructive to consider the total error possible in a residual stress measurement due to all the factors discussed. Samples cir-culated to many investigators can give perhaps the best view of the combined accuracy and precision to be expected. The following data is taken from ref. 28. The two tilt method was employed, with steel specimens.

1. SAE Round Robin No. 3 (11 laboratories reported, 1959)

    a. flat specimen (broad peak)

        stress level: 14 MPa

        standard deviation among laboratories: $\pm$ 10.3 MPa

    b. 1010 annealed flat steel (sharp peak)

        stress level: -5 MPa

        standard deviation: $\pm$ 16.5 MPa

2. SAE Round Robin No. 4 (25 laboratories, including many with little or
    no experience in residual stress measurements)

    a. flat, shot-peened (R_c 63)

    stress level: 593 MPa

    standard deviation: $\pm$ 41 MPa

    b. 1045 Round bar, 6.22 cm diameter (R_c 61/62)

    stress level: 910 MPa

    standard deviation (axial direction): $\pm$ 56.5 MPa

    standard deviation (longitudinal direction): $\pm$ 72 MPa

8. Acknowledgements

References

1. James, M. R. and Cohen, J. B.; "The measurement of residual stresses by X-ray diffraction techniques"; Experimental Methods in Materials Science, Vol. 1; H. Herman, ed.; (Academic Press, in press).

2. James, M. R. and Buck, O.; "Quantitative nondestructive measurements of residual stresses"; Critical Reviews in Solid State and Materials Science; in press).

3. Lester, H. H. and Aborn, R. H.; "Behavior under stress of the iron crystals in steel"; Army Ordnance; Vol. 6; 120-127, 200-207, 283-287, 364-369; (1925).

4. Evenschor, P. D. and Hauk, V.; "Über nichtlineare Netalbenenabstandsver- teilungen bei röntgenographischen Dehnungsmessungen"; Z. Metallkde.; 66; [3]; 167-168; (1975).

5. Dölle, H.; "Influence of multiaxial stress states, stress gradients and elastic anisotropy on the evaluation of (residual) stresses by X-rays"; J. Appl. Cryst.; in press.

6. Nye, J. F.; Physical Properties of Crystals; (Clarendon Press, Oxford, 1975).

7. James, M. R. and Cohen, J. B.; "PARS - a portable X-ray analyzer for residual stresses", J. of Testing and Evaluation; Vol. 6; [2]; 91-97; (1978).

8. Steffen, D. A. and Ruud, C. O.; "A versatile position sensitive X-ray detector"; Advances in X-ray Analysis, Vol. 21; eds. H. F. McMurdie, C. S. Barrett, J. B. Newkirk and C. O. Ruud; 309-315; (Plenum Press, New York, 1978).

9. Marion, R. H. and Cohen, J. B.; "The need for experimentally determined X-ray elastic constants"; Advances in X-ray Analysis, Vol. 20; eds. H. F. McMurdie, C. S. Barrett, J. B. Newkirk and C. O. Ruud; 355-367;

(Plenum Press, New York, 1977).

10. Prevey, P. S.; "A method of determining the elastic properties of alloys in selected crystallographic directions for X-ray diffraction residual stress measurements"; Advances in X-ray Analysis, Vol. 20; eds. H. F. McMurdie, C. S. Barrett, J. B. Newkirk and C. O. Ruud; 345-354; (Plenum Press, New York, 1977).

11. Dölle, H. and Cohen, J. B.; "Residual stresses in ground steels"; submitted for publication.

12. Walburger, H.; Conference On Residual Stress Analysis; Plättig, Germany, May 3/4.; (1973).

13. Dölle, H. and Hauk, V.; Röntgenographische Spannungsermittlung für Eigenspannungsysteme allgemeiner Orientierung; Härterei-Techn. Mitt.; 31; [3]; 165-169; (1976).

14. Murakami, M.; "Residual strains of Pb thin films deposited onto Si substrates"; Acta Met.; 26; 175-183; (1978).

15. Wolfstieg, U.; "Röntgenographische Spannungsmessungen mit breiten Linien"; Arch. Eisenhüttenwes; Vol. 30; 447-450; (1959).

16. Macherauch, E. and Wolfstieg, U.; "A modified diffractometer for X-ray stress measurements"; Advances in X-ray Analysis, Vol. 20; eds. H. F. McMurdie, C. S. Barrett, J. B. Newkirk and C. O. Ruud; 369-378; (Plenum Press, New York, 1977).

17. Schwartz, L. H. and Cohen, J. B.; Diffraction from Materials; (Academic Press, New York, 1977).

18. Chrenko, R. H.; "X-ray residual stress measurements using parallel beam optics"; Advances in X-ray Analysis, Vol. 20; eds. H. F. McMurdie, C. S. Barrett, J. B. Newkirk and C. O. Ruud; 393-402; (Plenum Press, New York, 1977).

19. James, M. R.; An Examination of Experimental Techniques in X-ray Residual Stress Analysis; Ph.D. Thesis; (Northwestern University, Evanston, IL., 1977).

20. Marion, R. H. and Cohen, J. B.; "Anomalies in measurement of residual stress by X-ray diffraction"; Advances in X-ray Analysis, Vol. 18; eds. W. L. Pickles, C. S. Barrett, J. B. Newkirk and C. O. Ruud; 446-501; (Plenum Publ. Co., New York, 1975).

21. Lecroisey, F., Miège, B. and Saint-Étienne, A.; La Mesure des Constraints Résiduelles: Method de Détermination par Rayons X; (Centre Techniques des Industries Mechaniques, B.P. 67, 60304 Senlis, France, 1978).

22. Marion, R. H.; X-ray Stress Analysis of Plastically Deformed Metals; Ph.D. Thesis; (Northwestern University, Evanston, IL., 1972).

23. Zantopulos, H. and Jatczak, C. F.; "Systematic errors in X-ray diffractometer stress measurements due to specimen geometry and beam divergence"; Advances in X-ray Analysis, Vol. 14; eds. C. S. Barrett, J. B. Newkirk and C. O. Ruud; 360-376; (Plenum Press, New York, 1971).

24. James, M. R. and Cohen, J. B.; "Study of the precision of X-ray stress analysis"; Advances in X-ray Analysis, Vol. 20; eds. H. F. McMurdie, C. S. Barrett, J. B. Newkirk and C. O. Ruud; 291-309; (Plenum Press, New York, 1977).

25. Koistinen, D. P. and Marburger, R. E.; "A simplified procedure for calculating peak position in X-ray residual stress measurements on hardened steel"; Trans. of the ASM; Vol. 51; 537-555; (1959).

26. Jingh, A. K. and Balasingh, C.; "Effect of X-ray diffractometer geometrical factors on the centroid shift of a diffraction line for stress measurement"; J. Appl. Physics; Vol. 42; [13]; 5254-5260; (1971).

27. James, M. R. and Cohen, J. B.; "The application of a position sensitive X-ray detector to the measurement of residual stresses"; Advances in X-ray Analysis, Vol. 19; eds. R. W. Gould, C. S. Barrett, J. B. Newkirk and C. O. Ruud; 695-708; (Kendall/Hunt Publ. Co., Dubuque, Iowa, 1976).

28. Residual Stress Measurement by X-ray Diffraction - SAEJ784a, eds. M. E. Hilley, J. A. Larson, C. F. Jatczak and R. E. Ricklefs; (Society of Automotive Engineers, Inc. Warrendale, PA., 1971).

Table I

The Influence of Various Mis-Alignments on the

Accuracy of Stress Analysis

+ = large error (0.07° or more)

- = small error (0.01° or less)

m = medium error

type of error	ψ tilt around θ axis	ψ tilt around axis in diffraction plane
centers of θ, ψ rotation not coincident ($\Delta = 0.1$ mm)	-	-
4° horizontal divergence	-	m
4° vertical divergence	m	-
1° horizontal tilt of beam to the zero direction	-	+
1° vertical tilt of beam to true zero direction	+	-
tube mis-alignment (Δx, Δy, $\Delta z \approx 1$ mm)	- + -	- - +
displacement of sample from the tilt axis (0.2 mm)	+	m to +
sample curvature (beam much smaller)	- to m	- to m

Table II

Typical Bias in Peak Location for $2\theta = 156^{\circ}$

(Approximately the 211 CrK_{α} Peak from Iron)

cause	peak shift between $\psi = 0^{\circ}$ and $\psi = 45^{\circ}$		peak shift between $\psi = 0^{\circ}$ and $\psi = 60^{\circ}$	
	$^{\circ}2\theta$	MPa	$^{\circ}2\theta$	MPa
peak location $\pm$ 0.01$^{\circ}2\theta$	+.02	11.9	$\pm$.02	$\pm$1700
total horizontal beam divergence of 1°	-.0006°	-0.35	-.0025	-215
vertical beam divergence[28] (assuming strong texture using divergent Soller slit; no receiving Soller slit)	$\pm$.002	$\pm$1.20	$\pm$.002	$\pm$170
sample displacement, $\Delta X' = \pm.025$ mm	$\pm$.0034	$\pm$2.1	$\pm$.0088	$\pm$760
ψ-axis displacement, $\Delta X' = \pm.025$ mm	$\pm$.002	$\pm$1.2	$\pm$.0068	$\pm$585
maximum total errors *+ a) in -2θ direction b) in +2θ direction	-.008 +.0068	-4.8 +4.1	-.0201 +.0149	-1150 +860

*Note: Maximum error is either one of these but not the total range.
+Calculated for steel from $\sigma_{\phi} = K_{\psi}$ $(2\theta-2\theta_{\phi})$ where $K_{45} = 602$ MPa/$^{\circ}2\theta$ and $K_{60} = 408.1$ MPa ksi/$^{\circ}2\theta$. Does not include error in peak location as it is dependent on time of data collection.

Table III

Precision of Various Measures of Profile Position

(10 measurements)

	Sample	Time (sec)	FWHM* ($^o2\theta$)	Half-Value Breadth ($^o2\theta$)	Centroid ($^o2\theta$)	Parabola ($^o2\theta$)
AISI	1090-1	50	.45	156.149 ($\pm$ .021)**	156.096 ($\pm$ .011)	156.186 ($\pm$ .016)
AISI	1045-2	100	3.45	155.336 ($\pm$ .064)	155.396 ($\pm$ .085)	155.413 ($\pm$ .020)

*FWHM is the full width at half of the maximum intensity

**The term in ( ) represents one standard deviation from the average position over the 10 measurements.

Figure Captions

Fig. 1   Top: Schematic of a diffractometer. The incident beam diffracts

from planes that satisfy Bragg's law, in grains with these planes paral-

lel to the sample's surface. If regions near the surface are in com-

pression, with the stress parallel to the surface, because of Poisson's

ratio, these planes are further apart than in the stress-free state.

The "d" spacing is obtained from the peak in intensity vs. scattering

angle 2θ (insert), and Bragg's law.

Bottom: After the specimen is tilted, diffraction occurs from other

grains, but from the same planes, and these are less separated than in

(a), because there is a component of the residual stress normal to the

planes.

Fig. 2   The axial system. The $\underline{L}_i$ are the laboratory system and measurements

of $\Delta d/d$ are made along L_3. The $\underline{P}_i$ describe the specimen.

Fig. 3   Interplanar spacing, "d", vs $\sin^2\psi$, normalized AISI-1010 steel,

deformed in tension along P_1 to a true strain of 8 pct. 211 peak,

CrK_α radiation; $\sigma_{\phi=0^o} = -107.1$ MPa (-15,303 psi). From ref. 22.

Fig. 4   The PARS system[7] - a portable (X-ray) analyzer for residual stresses.

A) linear position sensitive detector to record the entire diffraction

profile without detector motion; B) air-cooled miniature X-ray tube

(50 kV, 2 mA); C) exit soller slits; D) rods to position unit with

respect to a specimen; E) one (of two) handles.

Fig. 5   Normalized plain carbon steel strip (0.6 wt pct carbon) ground under

flowing water to remove 5 μm per pass[11]. Various ϕ tilts shown.

The curves are fits to the data points with eqn. (1). The stress

tensor in MPa is

$$\begin{pmatrix} 390 & 14 & 63 \\ 14 & 306 & -1 \\ 63 & -1 & 92 \end{pmatrix}$$

211 peak, CrK_α radiation.

Fig. 6 $\langle \epsilon'_{33} \rangle$ vs $\sin^2\psi$. Normalized plain carbon steel strip (0.6 wt pct carbon) ground to remove 5 μm per pass under flowing water[11]. $\bar\Phi = 0°$. Strain in units of 10^{-3}. Specimen C2 was ground only in the direction of the $+P_1$ axis. For specimen C5, the direction of grinding was reversed each pass with the final pass opposite to that for C2 (in the $-P_1$ direction). The stress tensor for C5 is given in Fig. 5. For C2 (in MPa) it is:

$$\begin{pmatrix} 199 & -10 & -63 \\ -10 & 86 & 5 \\ -63 & 5 & 84 \end{pmatrix}$$

Note that the curvature for $\psi > 0$, $\psi < 0$ reverses when σ_{13} reverses. The curves are the fits to the data points with the stress tensors and Eqn. 1. O: $\psi < 0$; ● $\psi > 0$.
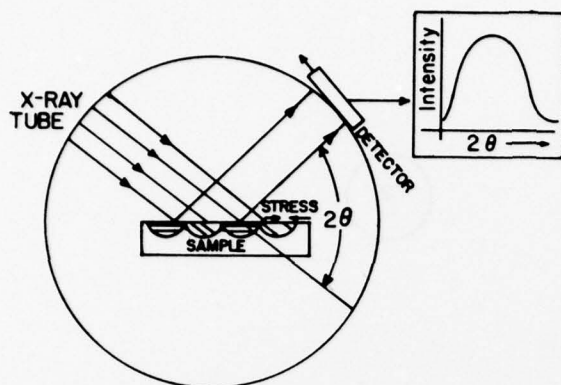
211 peak, CrK_α radiation

Fig. 7 Interplanar spacing, "d", vs $\sin^2\psi$ for a Cu_3Au, specimen pulled in tension along P_1 to a true strain of 35 pct[22], 420 peak, CuK_α radiation. The term $f(0,\psi)$ is the area under the Bragg peak at each ψ position.
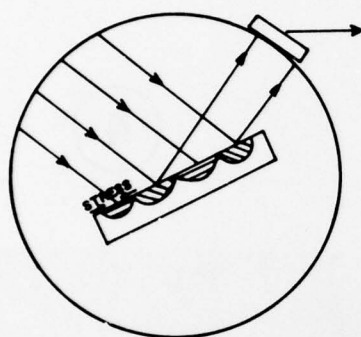
Fig. 8 The effect of various gradients on "d" vs $\sin^2\psi$. The gradient is assumed to be linear over the X-ray beam's depth of penetration, with slope g_{ij}. Typical values were assumed (for σ_{11}, 200-600 MPa over 20 μm, for σ_{33}, 100 MPa per μm, (zero at the surface)).
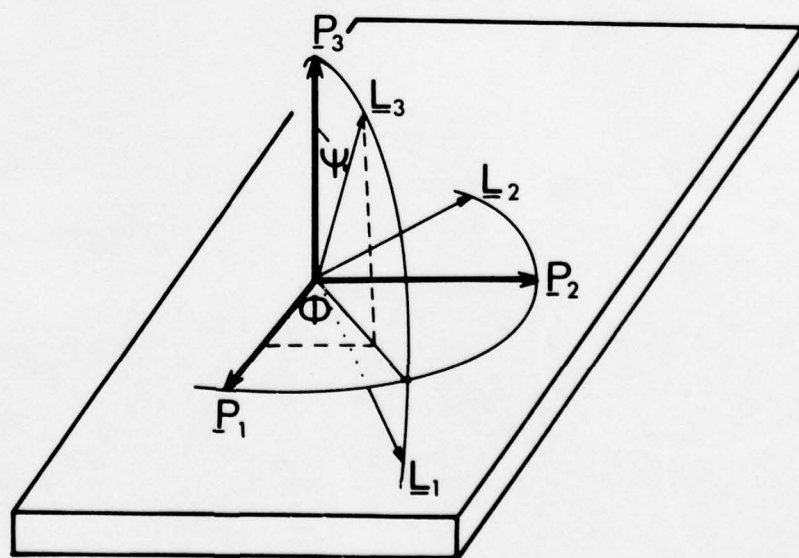
Fig. 9 Measured "d" vs $\sin^2\psi$, shot peened (normalized) AISI 1040 steel; data averaged over nine specimens. Error bars from observed variation in 2θ in repeated measurements. CoK_α, 310 reflection.

Fig. 10 a) The gradient measured by layer removal for one of the specimens in Fig. 9 (Etchant: 100 parts 30 pct H_2O, 10 parts 48 pct HF). Data uncorrected for layer removal and depth of penetration. 310 peak, CoK_α radiation.

b) Assumed gradients for calculations described in text to fit data in (a).

Fig. 11 The effect of sample displacement on "d" vs $\sin^2\psi$. Measurements made with an annealed Cr powder painted on a steel specimen in an acetone solution. 211 reflection, CrK_α radiation.

Fig. 12 Measured effects of sample displacement, for various focussing techniques employed in stress measurements. Normalized 1045 steel, 211 reflection, CrK_α radiation.

Fig. 13 Calculated peak shift due to $K_{\alpha_1} - \alpha_2$ doublet for various definitions of the peak

a) Special slits to symmetrize peak (Wolfstieg, U., Die Symmetrisierung unsymmetrischer Interferenzlinien mit Hilfevon, Spezial Henden, Härterei-Techn. Mit. 31, 23-26, (1978)).

b) center of gravity

c) middle of half-width

d) parabolic fit to top 15 pct

The same Gaussian functions were assumed for the α_1, α_2 components. 211 reflection, CrK_α radiation

Fig. 14 a) Precision of peak location (parabolic fit, top 15 pct). 572 peaks; actual standard deviations when the indicated precision was requested.

b) 440 peaks each examined 4 times; indicating the spread in each of these 4 repeated measurements.

Armco iron and steels, 211 reflection, CrK_α radiation.
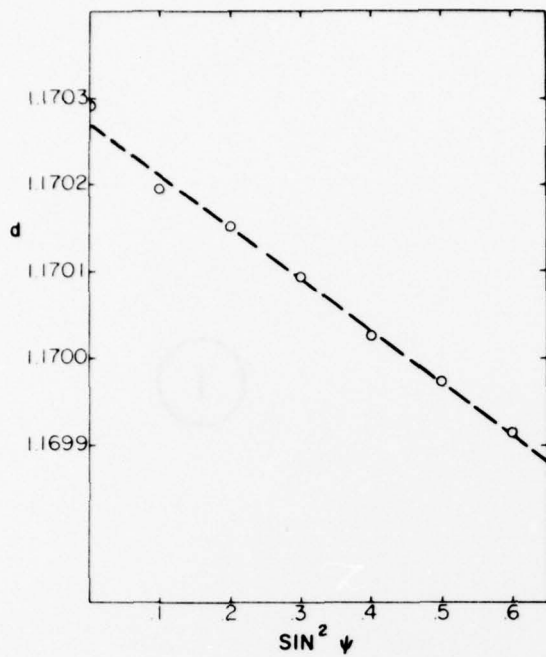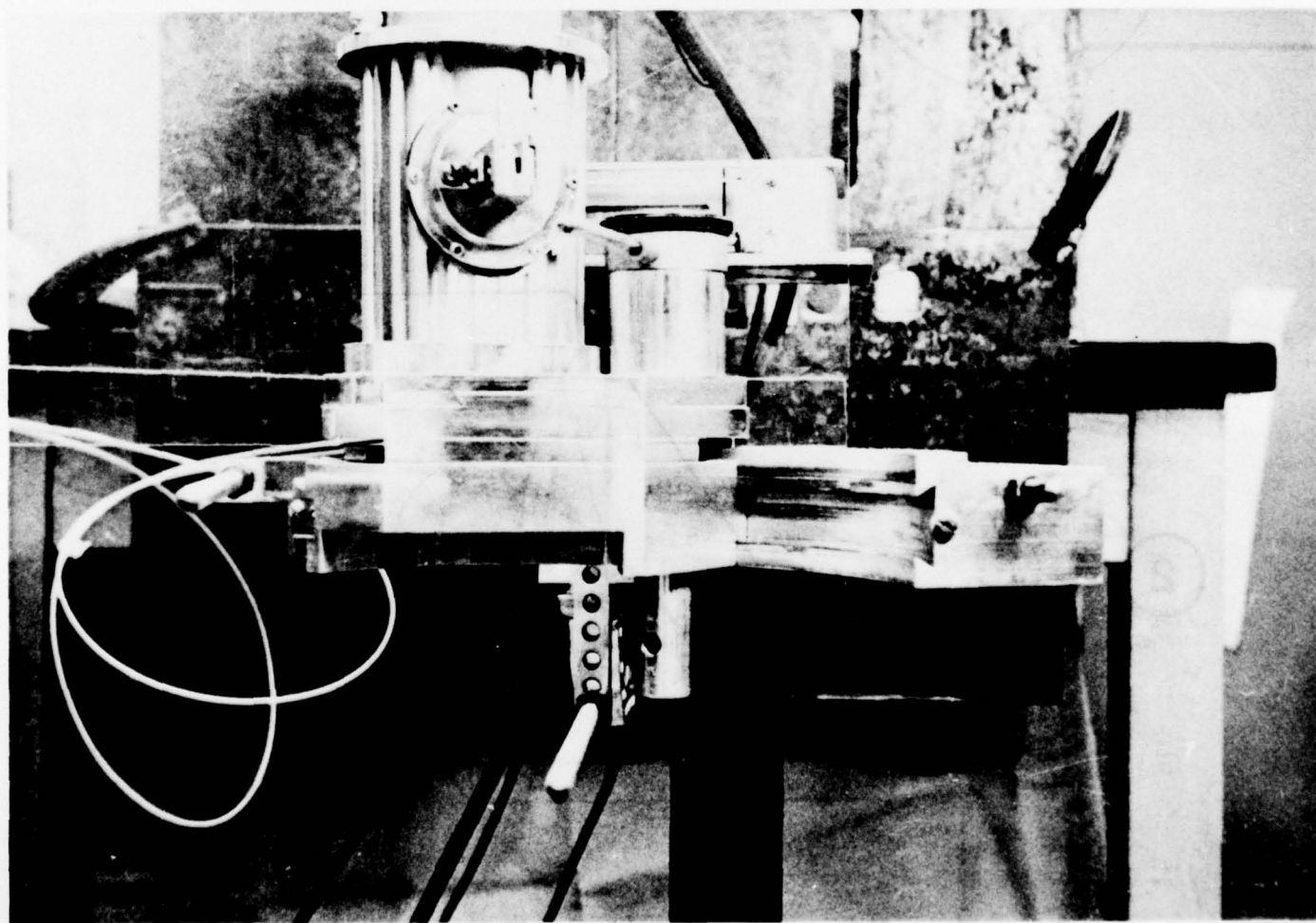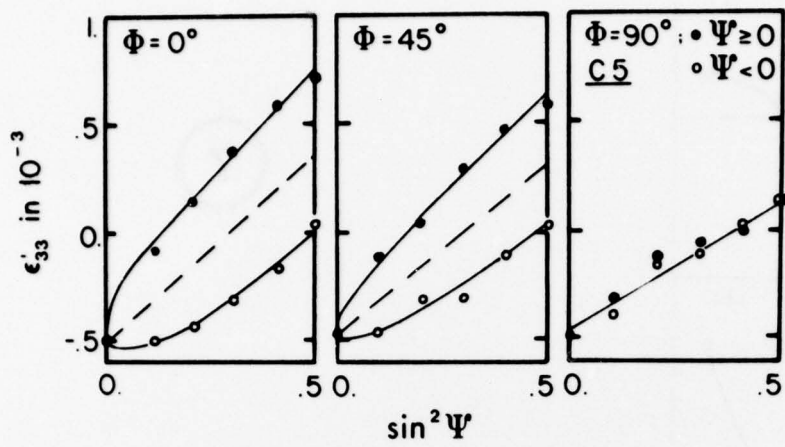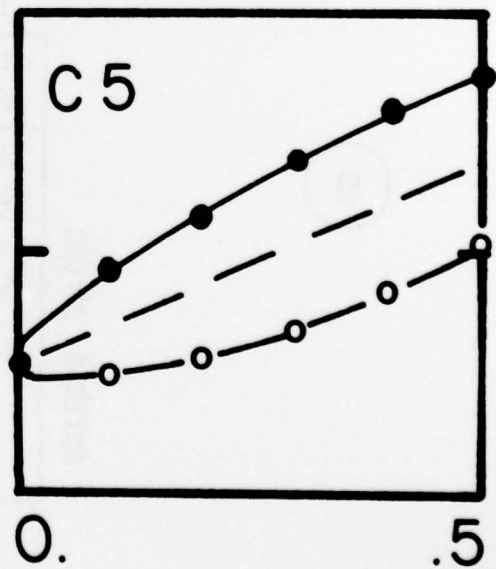7 point parabolic fit for peak positions.

X-RAY
TUBE

DETECTOR

Intensity

2θ

STRESS

2θ

SAMPLE

STRESS

①

②

$\underline{P}_3$

$\underline{L}_3$

ψ

$\underline{L}_2$

$\underline{P}_2$

Φ

$\underline{P}_1$

$\underline{L}_1$

$SIN^2 \psi$

ϵ'_{33} in 10^{-3}

$\Phi=0°$

$\Phi=45°$

$\Phi=90°$: $\bullet \Psi' \geq 0$
C 5 $\circ \Psi' < 0$

1.

.5

0

-.5

0.   .5 0.   .5 0.   .5

$\sin^2 \Psi'$

(5)

(6)

$\epsilon'_{33}(\Phi=0)$

1.

0.

-1.

C 2

C 5

0.   .5

0.   .5

(a)

.8381

.8380

d

.8379

.8378

(b)

1.0
.9
.8
.7
.6
$f(0,\psi)$
.5
.4
.3

.1   .2   .3   .4   .5

$SIN^2 \psi$

⑦

⑧

Type 1		Type 2		Type 3		Type 4	
$<\sigma_{11}>$	<0	$<\sigma_{11}>$	<0	$<\sigma_{11}>$	>0	$<\sigma_{11}>$	>0
$<g_{11}>$	<0	$<g_{11}>$	>0	$<g_{11}>$	<0	$<g_{11}>$	>0
$<\sigma_{33}>$	>0	$<\sigma_{33}>$	>0	$<\sigma_{33}>$	<0	$<\sigma_{33}>$	<0
$<g_{33}>$	>0	$<g_{33}>$	<0	$<g_{33}>$	>0	$<g_{33}>$	<0

lattice strain

$sin^2 \Psi$

.908

.907

d_{310} in Å

.906

0.

.5

$\sin^2 \Psi$

9

stress in MPa

removed layer in mm

10 a

$z_1 = 0$ ← z_2 → z_3

stress in MPa

$\sigma_{33}(z)$

$\sigma_{11}(z) = \sigma_{22}(z)$

depth

10 b

.2

S = .6 mm

S = 0.

$\Delta(2\Theta)$ in degrees

● $\Psi° \geq 0$
○ $\Psi° < 0$
— calculated

-.2

0.

$\sin^2 \Psi°$

.5

11

KSI
50

40

parafocusing

parallel
beam

30

STRESS

stationary
slit

20

10

0

-.08 -.06 -.04 -.02 .00 .02 .04 .06 .08

DISPLACEMENT
(inches)

12

Δ(2θ) in degrees

.5

.25

0.

a

b

c

d

1   2   3   4

half-width of doublet
in degrees

standard deviation in 10^{-2} degrees in 2θ

(14a)

(14b)

standard deviation in 10^{-2} degrees in 2θ
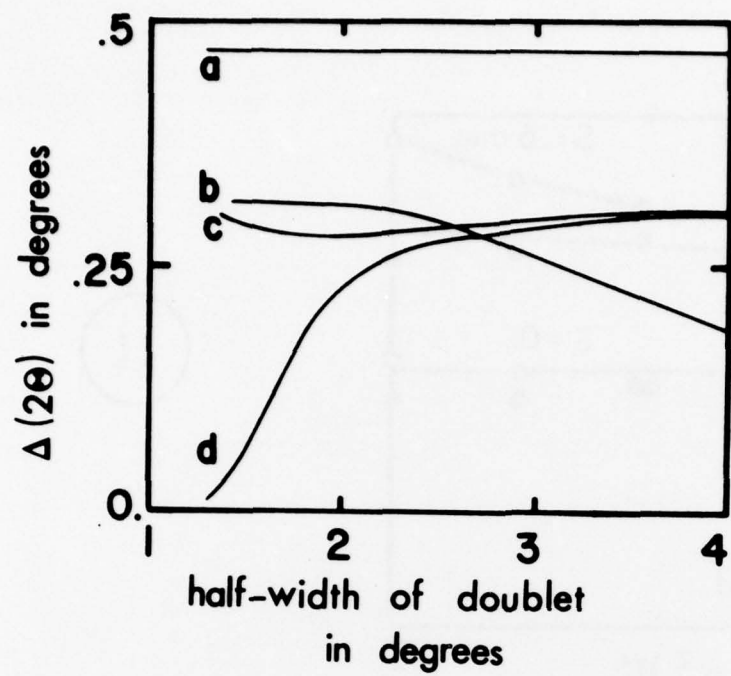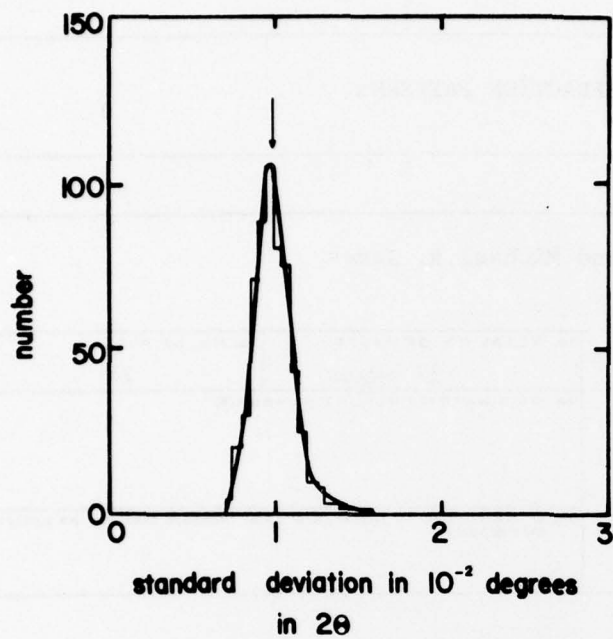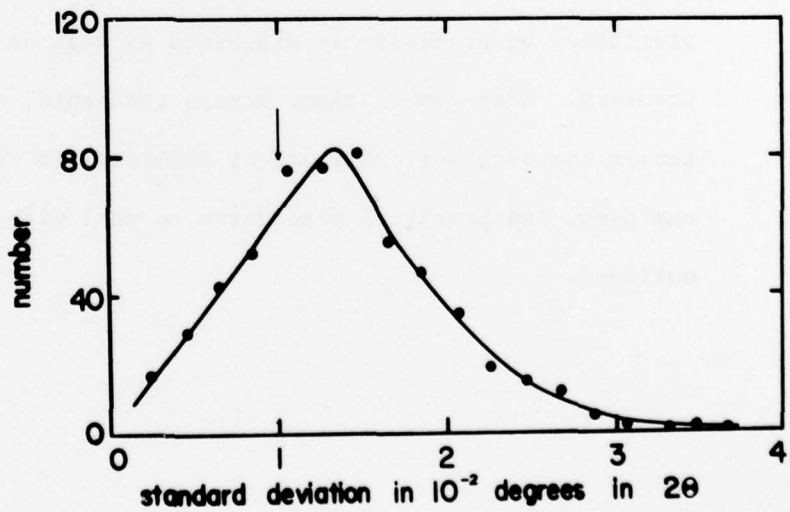
DOCUMENT CONTROL DATA - R & D

(Security classification of title, body of abstract and indexing annotation must be entered when the overall report is classified)

1. ORIGINATING ACTIVITY (Corporate author)	2a. REPORT SECURITY CLASSIFICATION
J. B. Cohen, Northwestern University Evanston, Illinois 60201	Unclassified
	2b. GROUP

3. REPORT TITLE

STRESS ANALYSIS FROM POWDER DIFFRACTION PATTERNS

4. DESCRIPTIVE NOTES *(Type of report and inclusive dates)*

Technical Report No. 23

5. AUTHOR(S) *(First name, middle initial, last name)*

Jerome B. Cohen, Heiner Dölle and Michael R. James

6. REPORT DATE	7a. TOTAL NO. OF PAGES	7b. NO. OF REFS
May 14, 1979	37 pages	28

8a. CONTRACT OR GRANT NO.	9a. ORIGINATOR'S REPORT NUMBER(S)
N00014-75-C-0580 P00005	
b. PROJECT NO.	
c.	9b. OTHER REPORT NO(S) (Any other numbers that may be assigned this report)
d.	

10. DISTRIBUTION STATEMENT

Distribution of this document is unlimited.

11. SUPPLEMENTARY NOTES	12. SPONSORING MILITARY ACTIVITY
	Metallurgy Branch Office of Naval Research

13. ABSTRACT

A brief review of the method of measuring residual stresses in polycrystalline materials with X-rays is given. The effect of counting statistics on precision is discussed as well as factors that affect accuracy. Beam penetration, stress gradients, and the form of the stress tensor can each seriously affect accuracy, if traditional methods are employed, and practical procedures to deal with such situations are outlined.

DD FORM 1 NOV 65 **1473** (PAGE 1)

S/N 0101-807-6801

14. KEY WORDS	LINK A		LINK B		LINK C	
	ROLE	WT	ROLE	WT	ROLE	WT
residual stresses, stresses, X-rays, diffraction						

DD FORM 1 NOV 65 **1473** (BACK)

(PAGE 2)